PCCP

ROYAL SOCIETY OF CHEMISTRY

PAPER

Cite this: *Phys. Chem. Chem. Phys.*, 2021, **23**, 17848

Study on the kinetics and dynamics of the H_2 + NH_2^- reaction on a high-level *ab initio* potential energy surface

Mengyi Pan,[ab] Haipan Xiang,[ab] Yong Li*[b] and Hongwei Song *[a]

Received 1st June 2021,
Accepted 28th July 2021

DOI: 10.1039/d1cp02423j

rsc.li/pccp

Gas-phase ion–molecule reactions play major roles in many fields of chemistry and physics. The reaction of an amino radical anion with a hydrogen molecule is one of the simplest proton transfer reactions involving anions. A globally accurate full-dimensional potential energy surface (PES) for the NH_2^- + H_2 reaction is developed by the fundamental invariant-neural network method, resulting in a root mean square error of 0.116 kcal mol^{-1}. Quasi-classical trajectory calculations are then carried out on the newly developed PES to give integral cross sections, differential cross sections and thermal rate coefficients. This reaction has two reaction channels, proton transfer and hydrogen exchange. The reactivity of the proton transfer channel is about one or two orders of magnitude stronger than that of the hydrogen exchange channel in the energy range studied. Vibrational excitation of H_2 promotes the proton transfer reaction, while fundamental excitation of each vibrational mode of NH_2^- has a negligible effect. In addition, the theoretical rate coefficients of the proton transfer reaction on the PES show inverse temperature dependence from 150 to 750 K, in accordance with the available experimental results.

I. Introduction

Gas-phase ion–molecule reactions play a pivotal role in many fields of chemistry and physics, such as interstellar chemistry, astrochemistry, plasma chemistry and combustion, which has attracted physicists as well as chemists to study their kinetics and dynamics.[1–10] This type of reactions usually have a large scattering cross section for inelastic or reactive processes due to the strong long-range interaction of the charged species with neutral atoms or molecules.[11–20]

Nitrogen is one of the six most abundant elements in the universe. The chemical network of nitrogen in the interstellar medium is still unclear due to the difficulty in observing key molecules from the ground.[21] Nitrogen hydrides are the precursors of the nitrogen chemical network, appearing in the first step of complex chain reactions. NH^+, an important species in nitrogen chemistry, is considered to be a potential candidate for detecting changes in the fine structure constant and the electron-to-proton mass ratio.[22] Another very interesting substance in nitrogen chemistry is the anion NH_2^-.[23] However, detection of NH^+ and NH_2^- is very difficult due to their low abundance and their strongest transitions being usually undetectable by ground-based telescopes.[23,24] Thanks to the launch of the high-resolution Herschel telescope and its sensitive far-infrared heterodyne instrument,[25,26] the average upper limit of NH^+ abundance was determined to be 10^{-10} at 4 K with respect to molecular hydrogen.[21] NH_2^- was also found to have very low abundance.[24]

The reaction of the amino radical anion NH_2^- with H_2, the most abundant molecules in the molecular cloud, is one of the simplest proton transfer reactions involving anions. This reaction is slightly exoergic and proceeds by overcoming a submerged barrier. The rate constant of the $H_2 + NH_2^- \rightarrow H^- + NH_3$ reaction was measured to be $(2.3 \pm 0.5) \times 10^{-11}$ cm^3 $molecule^{-1}$ s^{-1} at 297 K by Bohme *et al.* using a flowing afterglow system, about 2 orders of magnitude below the capture limit.[27] Otto *et al.* carried out an experimental study on the low-temperature reaction dynamics of $H_2 + NH_2^- \rightarrow H^- + NH_3$ in a 22-pole radiofrequency ion trap.[28] They found that the rate coefficient shows inverse temperature dependence from 300 to 20 K, in accordance with the longer life time of an intermediate complex, and it drops as the temperature further decreases, implying the presence of a very small barrier at long range or a quantum mechanical resonance.[28] Theoretically, Gianturco *et al.* reported the reaction rates at interstellar temperatures using the variational transition-state theory (VTST) approach.[29] The low temperature experimental data down to 8 K were well described by introducing a temperature-dependent factor in the VTST theory.

In this work, a full-dimensional, globally accurate potential energy surface (PES) for the $H_2 + NH_2^-$ reaction is developed by

[a] *State Key Laboratory of Magnetic Resonance and Atomic and Molecular Physics, Wuhan Institute of Physics and Mathematics, Innovation Academy for Precision Measurement Science and Technology, Chinese Academy of Sciences, Wuhan 430071, China. E-mail: hwsong@wipm.ac.cn*

[b] *College of Physical Science and Technology, Huazhong Normal University, Wuhan 430079, China. E-mail: yongli@mail.ccnu.edu.cn*

fitting ~46 000 *ab initio* points calculated at the level of CCSD(T)-F12a/aug-cc-pVTZ[30,31] and using the fundamental invariant-neural network method.[32] The dynamics and kinetics of the reaction are then investigated on the new PES using the quasi-classical trajectory (QCT) method.

II. Potential energy surface

The accuracy of a PES is generally determined by three factors: the *ab initio* method, the sampling scheme and the fitting (or interpolation) method. Much attention should be paid to the three aspects. Next, we introduce how to implement our solutions.

First, determination of the *ab initio* method/basis set: The geometries of stationary points along the minimum energy path (MEP) are optimized at the level of CCSD(T)-F12a/aug-cc-pVTZ using Molpro 2012 software.[33] Then, the energies of these geometries are computed at different levels of the methods/basis sets, including CCSD(T)/aug-cc-pVTZ, CCSD(T)-F12a/aug-cc-pVTZ, CCSD(T)-F12b/aug-cc-pVTZ, CCSD(T)/aug-cc-pVQZ and CCSD(T)/aug-cc-pV5Z, and listed in Table 1. To balance the accuracy and computational cost, CCSD(T)-F12a/aug-cc-pVTZ is employed in the following single point energy calculations.

Second, sampling data points: First of all, 2-dimensional (2D) grid points along the minimum energy path and its tangential direction are generated with the energy spanning roughly 75 kcal mol^{-1} from −15 to 60 kcal mol^{-1} with respect to the reactant asymptote. For the 2D grid points, the reactants are initiated from a separation of 30 Å and the products are ended with a separation of 20 Å. From each grid point, a trajectory is launched by Atom Centered Density Matrix Propagation (ADMP), implemented by Gaussian 09, Revision E.01[34] at the level of B3LYP/6-311G*. From these ADMP trajectories, the first batch of data points is sampled to generate the initial data set. This data set is then used to generate a raw PES. Starting from the raw PES, batches of quasi-classical trajectories are run from different initial conditions. New points from these trajectories whose geometries are not close to the existing data set are selected by using the Euclidean distance, which is defined as $\chi = \sqrt{\sum_{i=1}^{10} \left|\vec{R}_i - \vec{R}_j\right|^2}$ (where, $\vec{R}_i$ and $\vec{R}_j$ represent the nuclear distance of the existing configuration in the data set and the new configuration, respectively). The permutationally equivalent points are also included in this screening. The points that satisfy $\chi > 0.08$ Å in the interaction region or $\chi > 0.2$ Å in the asymptotic region are preserved. These new data points are added to the previous data set to repair the non-physical region of the raw PES. After a new batch of points is added to the data set, a new PES, which is expected to be better than the previous one, is produced. This procedure is repeated dozens of times, like the GROW procedure.[35] Finally, a total of 45 932 data points are kept in the data set.

Third, fitting the data set: The fundamental invariant-neural network (FI-NN)[36] method is utilized to fit the data set. This method not only has the flexibility of the neural network (NN),[37] but also keeps the permutation invariant by introducing the fundamental invariant polynomials (FIs) into the NN as input.[32,38,39] Theoretically, as long as enough data points are sampled in the relevant configuration space, the NN fitting can approximate any function to any accuracy.[37] The Morse-like variables $P_{ij} = \exp(-r_{ij})$ are used to construct the polynomials, in which r_{ij} is the nuclear distance between the ith and the jth atoms.[40] For the AB_4 molecule system, the number of fundamental invariant polynomials is 31, with a maximum degree of 4. The architecture of NN is 31–30–30–1, giving a total of 1925 parameters. The input layer has 31 invariant polynomials, the two hidden layers have 30 and 30 neurons, and the output layer has 1 potential energy. All fittings are carried out using the Levenberg–Marquardt algorithm.[40] The root mean square error (RMSE), defined as $\mathrm{RMSE} = \sqrt{\sum_{i=1}^{N_{\mathrm{data}}} (E_{\mathrm{fit}} - E_{\mathrm{ab\,initio}})^2 \Big/ N_{\mathrm{data}}}$, is employed to assess the quality of each fitting. The data set is randomly divided into two groups, with 95% of the points as the training set and 5% as the validating set. The fits with the two sets having small and close RMSEs are considered to be acceptable. In addition to the RMSE, the final PES is also checked for other aspects, such as smoothness, structure, energies and frequencies of the stable points along the minimum energy path, energy conservation during QCT propagations and so on. Finally, the so-called ensemble approach is used to minimize random errors.[41] The total RMSE of the final PES is 0.116 kcal mol^{-1}, which is the average of two PESs with the training/validating RMSEs of 0.111/0.328 and 0.116/0.241 kcal mol^{-1}, respectively.

III. Quasi-classical trajectory method

The standard QCT calculations are implemented using the software VENUS 96.[42] By calling the subroutine of the newly developed FI-NN PES, the integral cross section (ICS) of the reaction is given by

$$\sigma_{\mathrm{r}}(E_{\mathrm{c}}) = \pi b_{\mathrm{max}}{}^2 \frac{N_{\mathrm{r}}}{N_{\mathrm{tot}}}, \quad (1)$$

where N_{r} and N_{tot} are the numbers of reactive and total trajectories at a specified collision energy E_{c}. The maximum impact parameter

Table 1 Energies (in kcal mol^{-1}) and CPU times (in min) of single-point energy calculations of stationary points along the minimum energy path at the CCSD(T) level in combination with different basis sets

	$NH_2^- + H_2$	$NH_2^-{\cdot}H_2$	TS1	$NH_3{\cdot}H^-$	$NH_3 + H^-$	Time
CCSD(T)/aug-cc-pV5Z	0.000	−4.280	−1.455	−14.623	−6.074	176
CCSD(T)/aug-cc-pVQZ	0.000	−4.354	−1.677	−14.837	−6.233	26
CCSD(T)/aug-cc-pVTZ	0.000	−4.423	−1.884	−15.114	−6.484	1.77
CCSD(T)-F12a/aug-cc-pVTZ	0.000	−4.432	−1.822	−15.001	−6.342	2.42
CCSD(T)-F12b/aug-cc-pVTZ	0.000	−4.435	−1.907	−15.184	−6.533	5.45

b_{max} is determined using small batches of trajectories with trial values at each specified collision energy. The impact parameter b is sampled by $b = R^{1/2}b_{max}$, in which R is a uniform random number in [0, 1]. The relative statistical error is defined by $\Delta = \sqrt{(N_{tot} - N_r)/N_{tot}N_r}$.

The differential cross section (DCS) is calculated by

$$\frac{d\sigma_r}{d\Omega} = \frac{\sigma_r P_r(\theta)}{2\pi \sin(\theta)}, \quad (2)$$

where the scattering angle θ is defined as

$$\theta = \cos^{-1}\left(\frac{\vec{v}_i \cdot \vec{v}_f}{|\vec{v}_i||\vec{v}_f|}\right), \quad (3)$$

in which $\vec{v}_i = \vec{v}_{NH_2^-} - \vec{v}_{H_2}$ and $\vec{v}_f = \vec{v}_{NH_3} - \vec{v}_{H^-}$ denote the initial and final relative velocities. The normalized probability $P_r(\theta')$ in eqn (2) is obtained by

$$P_r(\theta') = \frac{\sum_{\theta \geq \theta' - \Delta\theta'}^{\theta < \theta' + \Delta\theta'} N_r(\theta)}{N_r}, \quad (4)$$

where $\Delta\theta'$ is taken as 5.0° in the calculations.

The rate coefficient at temperature T is calculated by

$$k(T) = \left(\frac{8k_B T}{\pi\mu}\right)^{1/2} \pi b_{max}^2 \frac{N_r}{N_{tot}}, \quad (5)$$

where μ is the reduced mass between the reactants NH_2^- and H_2, and k_B is the Boltzmann constant. At each specific temperature T, the initial rovibrational energies of the two reactants and the collision energy are sampled according to the Boltzmann distribution.

In dynamics calculations, trajectories are initiated from a reactant separation of 30 Å and ended when the separation of products for reactive trajectories or reactants for nonreactive trajectories is larger than 20 Å. The time step is set as 0.05 fs, which conserves the energy better than 10^{-4} kcal mol^{-1} in the propagation. For each initial state, 30 000–80 000 trajectories are dispatched, giving the relative statistical errors all below 2%.

IV. Results and discussion

A. Properties of potential energy surface

Fig. 1a shows the schematic diagram of the reaction path for the proton transfer channel $NH_2^- + H_2 \rightarrow NH_3 + H^-$. The *ab initio* energy at the CCSD(T)-F12a/aug-cc-pVTZ level, the fitted energy, and the zero-point energy (ZPE) corrected energy of each stationary point along the reaction path are listed in the figure as well. Clearly, all stationary structures have a C_S symmetry. There exists a submerged barrier TS1, whose energy is slightly lower than that of the reactant asymptote by 1.854 kcal mol^{-1}. The reaction appears to occur as follows: the reactants encounter to form a metastable complex $NH_2^-{\cdot}H_2$, a proton in the H_2 moiety is then transferred to the NH_2^- moiety by overcoming the transition state TS1, a highly excited ammonia hydride complex, $NH_3{\cdot}H^-$, is formed and eventually this dissociates into products. Interestingly, there exists another transition state TS2

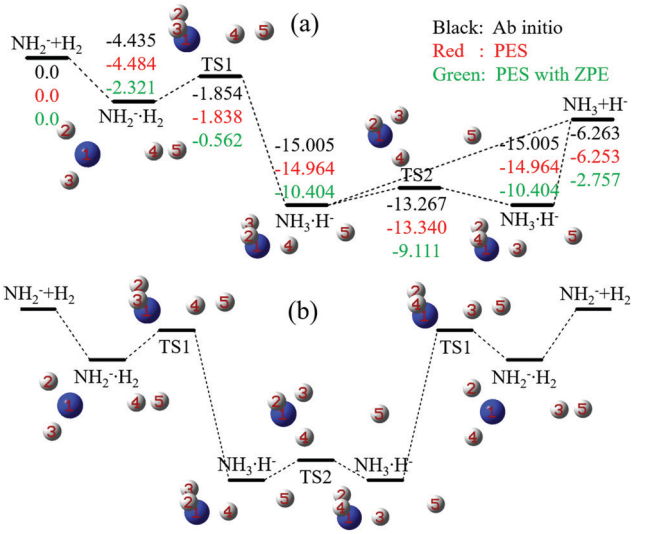

Fig. 1 Schematic diagram of the reaction paths for the NH_2^- + H_2 reaction. The *ab initio* energies of stationary points at the level of CCSD(T)-F12a/aug-cc-pVTZ (black); the values on the fitted PES (red) and the zero-point energy corrected values (blue) are shown below the corresponding geometries. All energies are given in kcal mol^{-1} and relative to the reactant asymptote. (a) Proton transfer channel; and (b) hydrogen exchange channel.

in the product well, corresponding to the rotation of H^- with respect to NH_3. In addition to the proton transfer channel, as shown in Fig. 1b, there exists another reaction channel, the symmetric hydrogen exchange channel $NH'H^- + H_2 \rightarrow NH_2^- + HH'$. In this channel, one of the hydrogen atoms in NH_2^- is exchanged with a hydrogen atom in H_2, caused by the rotation of H^- around NH_3 in the central deep well. The reaction path of the proton transfer channel is similar to the back-side attack pathways of the S_N2 reactions $NH_2^- + CH_3Y$ [Y = F, Cl, Br, I].[43] There also exist two submerged barriers for the back-side attack pathway. In contrast to the proton transfer pathway, the height of the pre-reaction TS in the S_N2 pathway is close to the height of the Walden TS.

Table 2 compares the geometries of the stationary points optimized at the level of CCSD(T)-F12a/aug-cc-pVTZ and on the PES. It can be seen that the difference between the fitted and *ab initio* values is less than 0.02 Å for each bond length and less than 2° for each angle. The bond distances of N1–H4 and H4–H5 optimized at the level of MP2/aug-cc-pVTZ by Gianturco *et al.* are presented in Table 2 as well.[29] The reported bond distances agree reasonably well with our results although TS2 was not obtained. The corresponding ZPE corrected energy of each stationary point at the level of CCSD(T)/aug-cc-pVTZ is also in good agreement with our results, shown in Fig. 1a. The energy difference is mostly less than 0.2 kcal mol^{-1}. Table 3 compares the fitted energies and harmonic frequencies of the stationary points with *ab initio* values. The fitting values, both energies and harmonic frequencies, are in good agreement with the *ab initio* calculations. The energy difference is all less than 0.07 kcal mol^{-1} and the frequency difference is largely smaller than 25 cm^{-1}. The maximum frequency deviation occurs for the reactant complex $NH_2^-{\cdot}H_2$, being 130 cm^{-1}. Overall, the PES reproduces well the properties of stationary points.

Table 2 Geometries (bond length in Angstrom and angle in degree) of the stationary points for the $NH_2^- + H_2 \rightarrow NH_3 + H^-$ reaction. The corresponding atom labels are shown in Fig. 1

Species	Method	$R_{N_1H_2}$	$R_{N_1H_3}$	$R_{N_1H_4}$	$R_{H_4H_5}$	$\theta_{H_2N_1H_3}$	$\theta_{H_2N_1H_4}$	$\theta_{N_1H_4H_5}$	$\varphi_{H_4N_1H_2H_3}$	$\varphi_{H_5H_4N_1H_2}$
NH_2^-	*Ab initio*[a]	1.029	1.029			102.00				
	PES	1.029	1.029			102.00				
H_2	*Ab initio*[a]				0.742					
	Ab initio[b]				0.737					
	PES				0.742					
$NH_2^-\cdot H_2$	*Ab initio*[a]	1.028	1.028	2.168	0.766	102.26	130.17	179.70	180.00	180.00
	Ab initio[b]			2.185	0.761					
	PES	1.028	1.028	2.176	0.765	102.37	128.82	180.00	180.00	180.00
TS1	*Ab initio*[a]	1.026	1.026	1.505	0.920	102.76	101.32	179.64	−104.51	52.83
	Ab initio[b]			1.475	0.926					
	PES	1.027	1.027	1.501	0.922	102.90	101.65	179.94	−104.99	53.15
$NH_3\cdot H^-$	*Ab initio*[a]	1.016	1.016	1.035	1.903	104.61	103.53	168.06	108.15	−54.48
	Ab initio[b]			1.041	1.818					
	PES	1.016	1.016	1.035	1.906	104.73	103.74	168.44	108.49	−54.61
TS2	*Ab initio*[a]	1.017	1.019	1.019	2.521	103.80	103.80	112.28	−102.62	96.24
	PES	1.017	1.019	1.019	2.540	104.00	104.00	112.40	−103.02	97.97
NH_3	*Ab initio*[a]	1.012	1.012	1.012		106.62	106.62		113.61	
	Ab initio[b]			1.013						
	PES	1.012	1.012	1.012		106.63	106.63		113.63	

[a] This work, CCSD(T)-F12a/aug-cc-pVTZ. [b] Ref. 29, MP2/aug-cc-pVTZ.

Table 3 Energies (in kcal mol^{-1}) and harmonic frequencies (in cm^{-1}) of the stationary points for the $NH_2^- + H_2 \rightarrow NH_3 + H^-$ reaction calculated at the level of CCSD(T)-F12a/aug-cc-pVTZ

			Frequency								
Species	Method	*E*	1	2	3	4	5	6	7	8	9
$NH_2^- + H_2$	*Ab initio*	0.0	4401	3377	3293	1489					
	PES	0.0	4398	3388	3293	1484					
$NH_2^-\cdot H_2$	*Ab initio*	−4.44	3967	3389	3304	1495	778	695	292	125	56i
	PES	−4.48	4005	3399	3306	1495	752	707	295	141	74
TS1	*Ab initio*	−1.85	3417	3326	1846	1510	1393	1284	409	373	856i
	PES	−1.84	3429	3314	1821	1508	1404	1286	420	371	881i
$NH_3\cdot H^-$	*Ab initio*	−15.01	3548	3474	3176	1698	1655	1214	421	383	307
	PES	−14.96	3544	3487	3164	1694	1640	1206	418	391	306
TS2	*Ab initio*	−13.27	3541	3497	3428	1670	1664	1235	335	234	279i
	PES	−13.34	3540	3495	3426	1676	1655	1231	345	253	251i
$NH_3 + H^-$	*Ab initio*	−6.26	3609	3609	3477	1673	1673	1055			
	PES	−6.25	3606	3606	3458	1675	1675	1064			

Fig. 2 shows the fitting errors of the sampled data points as a function of energy. The fitting error is defined as the deviation of fitted energy from the corresponding *ab initio* energy. The error points are dominantly distributed in between −0.5 and 0.5 kcal mol^{-1} and centered at 0 over the whole energy range. Very few points are scattered within [−0.5, −1.0] and [0.5, 1.0]. This distribution indicates that the FI-NN method has good flexibility to represent the PES. Fig. 3 displays the contours of the PES as a function of bond lengths of the breaking bond H–H′ and the forming bond N–H with the other internal coordinates fixed at the geometry of TS1. It can be seen from the figure that the PES is smooth without any artificial pits. The existence of any other artificial pits is excluded by plotting the contours along different dimensions. The pre- and post-reaction wells and submerged barrier are shown in the inset.

The MEP of the $NH_2^- + H_2 \rightarrow NH_3 + H^-$ reaction along the reaction coordinate *s* on the PES is depicted in Fig. 4, which is

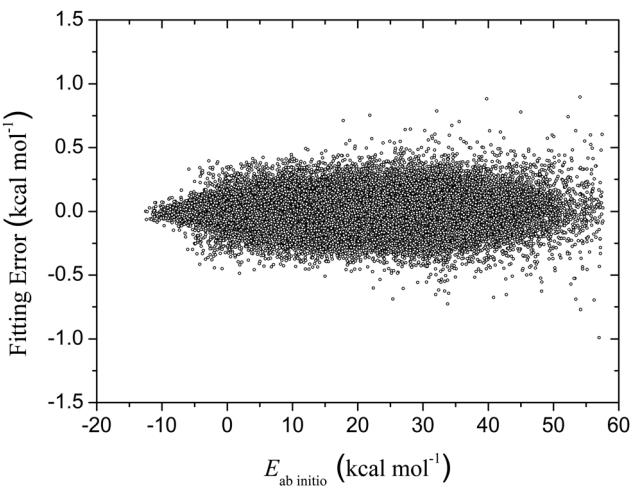

Fig. 2 Fitting errors ($E_{fit} - E_{ab\ initio}$) as a function of energy.

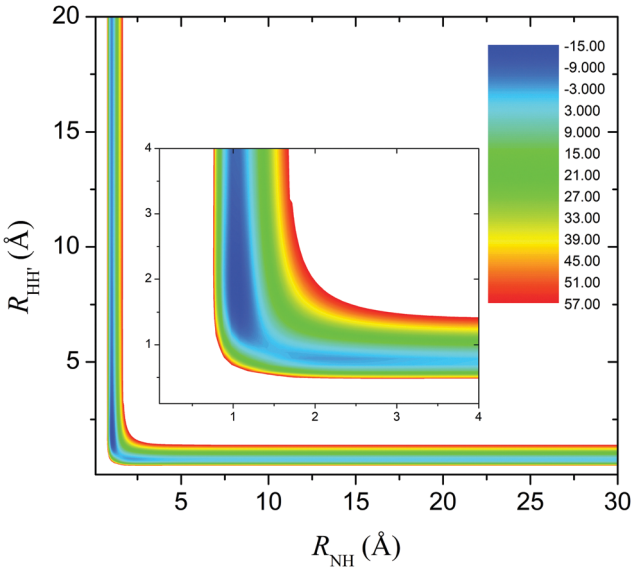

Fig. 3 Contours of the PES as a function of bond lengths of the breaking NH and the forming HH′ with the other coordinates fixed at the transition state. The energy is taken from −15.0 to 60.0 kcal mol^{-1}.

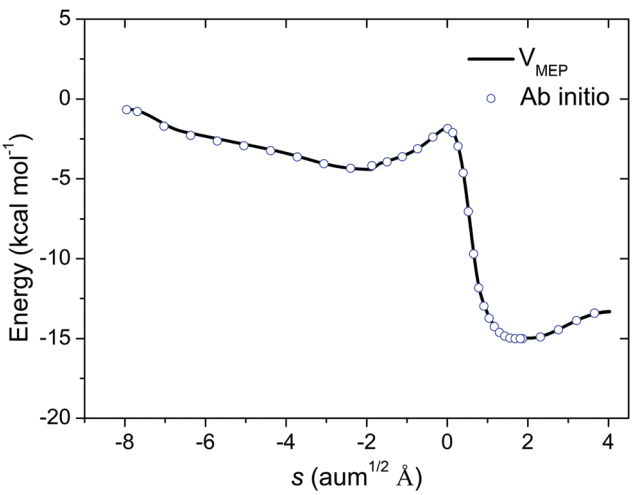

Fig. 4 Comparison of the fitted (solid line) and *ab initio* (circle) minimum energy paths for the $NH_2^- + H_2 \rightarrow NH_3 + H^-$ reaction. The *ab initio* energies are calculated at the level of CCSD(T)-F12a/aug-cc-pVTZ.

obtained by using the software Polyrate 9.7.[44] The reaction coordinate s is defined as the signed distance from the saddle point ($s = 0$), where $s > 0$ represents the product side and $s < 0$ denotes the reactant side. In order to further assess the accuracy of the PES, some geometries along the MEP are selected, followed by single point energy calculations at the level of CCSD(T)-F12a/aug-cc-pVTZ. Obviously, the MEP on the PES agrees well with the *ab initio* calculation. The Fortran subroutine of the PES is available at https://github.com/apmtcc/NH4ion.

Mazo-Sevillano *et al.* showed that the non-linearity of the transfer function employed in the NN fitting introduces spurious long-range interactions between reactants (or products).[45] These spurious interactions possibly have a remarkable effect on dynamics at low collision energies. Fig. 5 compares the fitted energy with the corresponding *ab initio* value with the reactants (or products) approaching along different orientations. Although the fitting errors are very small, the fitted PES cannot reproduce well the weak long-range attraction interaction. When the separation of the two reactants (or products) is larger than about 10 Å, the fitted PES becomes nearly distance independent. The unreasonable long-range interaction in the fitting is not likely to be caused by the non-linearity of the transfer function. It possibly originates from the Morse-like variables $P_{ij} = \exp(-r_{ij}/\alpha)$ used to construct the FI polynomials. In this work, α was taken as 1 because it gave a small RMSE of fitting. The variation of bond distance at large separation, however, cannot be reflected by the employed Morse-like variables. Adjusting the parameter α possibly improves the performance at long distances, but the price is the increase of the RMSE of the resulting PES. Since the long-range interaction is critical to low-energy collisions, one should be cautious when applying this PES to study collisions at ultracold temperatures.

B. Dynamics and kinetics

Fig. 6 shows the calculated ICSs from the reactant ground and fundamental states. PT denotes the proton transfer channel and HE refers to the hydrogen exchange channel in the figure.

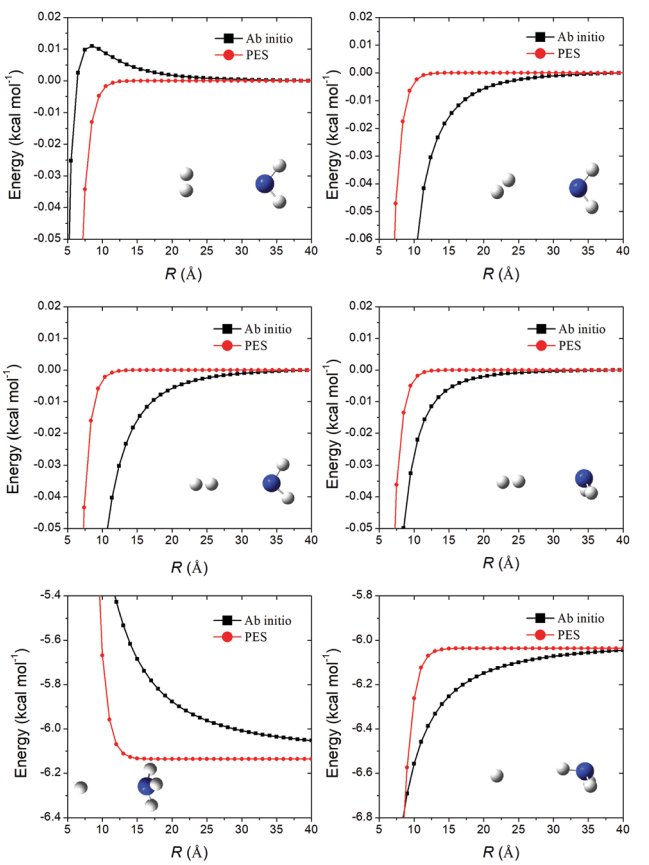

Fig. 5 Comparison of the fitted and *ab initio* energies with the reactants (or products) approaching along different orientations. The *ab initio* energies are calculated at the level of CCSD(T)-F12a/aug-cc-pVTZ.

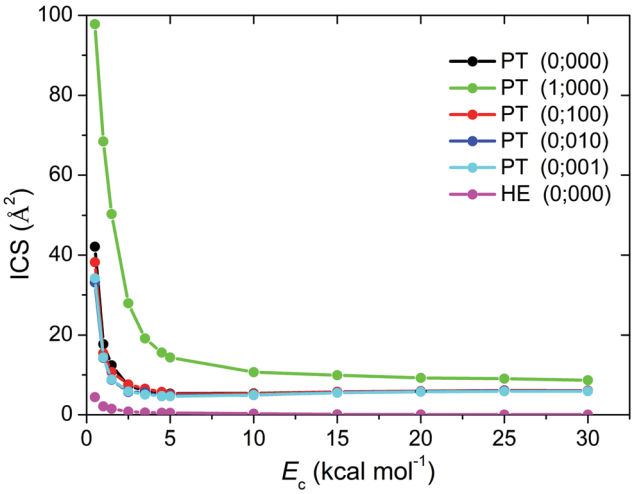

Fig. 6 Integral cross sections of the NH_2^- + H_2 reaction from the ground and excited vibrational states of the fundamental vibrational frequencies of the reactants NH_2^- and H_2. PT denotes the proton transfer channel and HE refers to the hydrogen exchange channel.

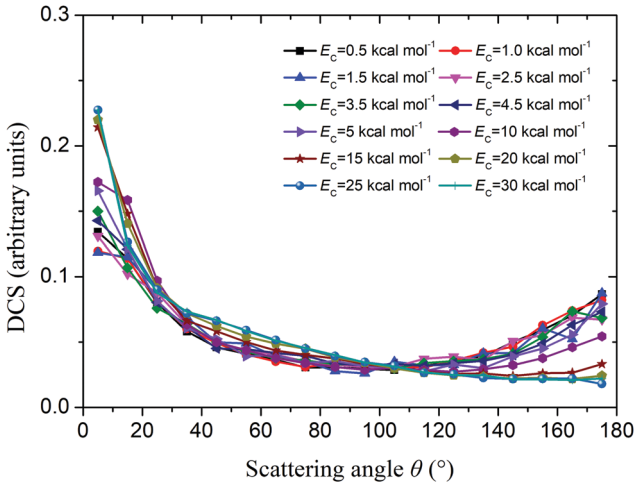

Fig. 7 Differential cross sections of the NH_2^- + H_2 → NH_3 + H^- reaction from the reactant ground state with the collision energy E_c fixed at 0.5, 1.0, 1.5, 2.5, 3.5, 4.5, 5.0, 10.0, 15.0, 20.0, 25.0 and 30.0 kcal mol^{-1}, respectively.

The initial vibrational states of the reactants H_2 and NH_2^- are labeled by v_{H_2}; v_1, v_2, and v_3, in which v_{H_2} represents the vibrational excitation in H_2, and v_1, v_2, and v_3 represent excitations in the symmetric stretching mode, the bending mode, and the antisymmetric stretching mode of NH_2^-, respectively. For both the proton transfer and hydrogen exchange channels, the ICS decreases rapidly at first with the increase in collision energy and then becomes nearly flat, which satisfies the character of barrier-less reactions. By contrast, the PT ICS is about one or two orders of magnitude larger than the corresponding HE value.

Since the reactivity of the hydrogen exchange channel is much lower than the proton transfer channel, the discussions hereafter focus on the proton transfer reaction. As shown in Fig. 6, excitation of the H_2 vibrational mode significantly enhances the proton transfer reaction at low collision energies below 5 kcal mol^{-1} and yet the enhancement effect becomes weak as the collision energy increases. This promotional effect is easily understood since the vibrational motion of H_2 is actually along the reaction coordinate. Excitation of each vibrational mode of NH_2^- has a negligible effect on the reaction, indicating that the vibrational motion of NH_2^- has little coupling with the reaction coordinate and thus its vibrational energy cannot flow into the reaction coordinate effectively.

Fig. 7 shows the differential cross sections (DCSs) of the NH_2^- + H_2 → NH_3 + H^- reaction from the reactant ground state with the collision energies at 0.5, 1.0, 1.5, 2.5, 3.5, 4.5, 5.0, 10.0, 15.0, 20.0, 25.0 and 30.0 kcal mol^{-1}, respectively. At low collision energies, the DCS has an approximate symmetric distribution, indicating that long-lived reaction intermediate(s) is(are) formed during the reaction. By checking the reactive trajectories, it is found that for most of the reactive trajectories the colliders are trapped in the product well with one of the dissociated H^- rotating around the NH_3 moiety. Thus, the reaction is dominated by the indirect mechanism. As the collision energy increases, the DCS starts to favor the forward and sideway scatterings, implying that the direct stripping mechanism becomes more and more important.

The calculated thermal rate coefficients of the NH_2^- + H_2 → NH_3 + H^- reaction on the PES are displayed in Fig. 8, together with available experimental and theoretical results. The corresponding values are listed in Table 4. As aforementioned, Otto *et al.* found that the measured rate coefficient has inverse temperature dependence between 300 to 20 K while has a positive correlation at temperatures from 20 to 8 K.[28] The theoretical rate coefficient obtained by the QCT method on the PES shows inverse temperature dependence from 150 to 750 K as well, although the theoretical value is about twice the corresponding experimental result. The difference is possibly caused by the inherent drawbacks of the QCT method, such as ZPE leakage and neglect of the quantum tunneling effect. By contrast, Gianturco *et al.*'s VTST values agree better with experimental measurements; however, a temperature-dependent

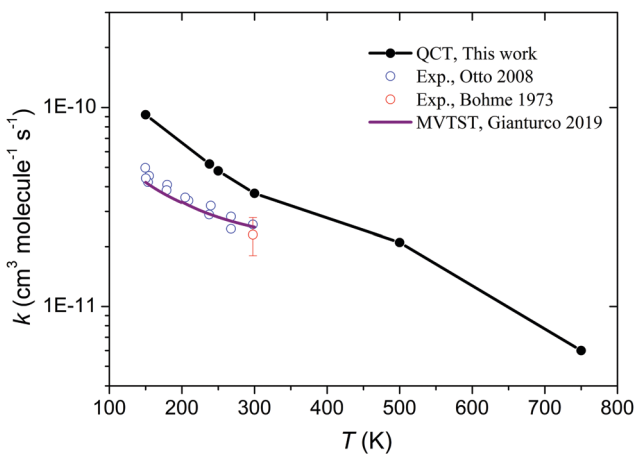

Fig. 8 Comparison of theoretical and experimental thermal rate coefficients for the NH_2^- + H_2 → NH_3 + H^- reaction.

Table 4 Thermal rate coefficients ($\times 10^{-11}$ cm^3 molecule^{-1} s^{-1}) for the $NH_2^- + H_2 \rightarrow NH_3 + H^-$ reaction

T (K)	QCT[a]	Exp.[b]	Exp.[c]
150	9.2		4.7
238	5.2		3.1
250	4.8		
300	3.7	2.3 ± 0.5	2.6
500	2.1		
750	0.6		

[a] QCT, this work. [b] Exp., see ref. 27. [c] Exp., see ref. 28.

factor must be introduced in the VTST theory. As the temperature drops down to below 150 K, the quantum effect is expected to be significant, and we thus don't carry out QCT calculations at these temperatures.

V. Conclusions

In this work, we construct an accurate full-dimensional *ab initio* PES for the $NH_2^- + H_2$ reaction with an RMSE of 0.116 kcal mol^{-1}. The FI-NN method is used to fit 45 932 energy points calculated at the level of CCSD(T)-F12a/aug-cc-pVTZ. The geometry, energy and harmonic frequencies of each stationary point along the minimum energy path reproduce the *ab initio* results well.

QCT calculations on the PES show that for both the proton transfer and hydrogen exchange channels the ICS first drops sharply and then becomes nearly flat with the increase in collision energy. The ICS of the hydrogen exchange reaction is about one or two orders of magnitude smaller than the corresponding proton transfer value. The proton transfer reaction is dominated by the indirect mechanism at low collision energies, while the direct stripping mechanism becomes more and more important as the collision energy increases. Vibrational excitation of the reactant H_2 significantly enhances the reaction. By contrast, exciting each of the vibrational modes of NH_2^- has a negligible effect on the reaction. The calculated rate coefficients of the $NH_2^- + H_2 \rightarrow NH_3 + H^-$ reaction on the PES show inverse temperature dependence from 150 to 750 K, in agreement with the available experimental results.

Conflicts of interest

There are no conflicts to declare.

Acknowledgements

This work was supported by the National Natural Science Foundation of China under Grant No. 21973109.

References

1 E. E. Ferguson, *Annu. Rev. Phys. Chem.*, 1975, **26**, 17–38.
2 W. D. Watson, *Acc. Chem. Res.*, 1977, **10**, 221–226.
3 D. Smith, *Chem. Rev.*, 1992, **92**, 1473–1485.
4 C.-Y. Ng, *J. Phys. Chem. A*, 2002, **106**, 5953–5966.
5 J. Mikosch, M. Weidemüller and R. Wester, *Int. Rev. Phys. Chem.*, 2010, **29**, 589–617.
6 A. Fridman, *Plasma Chemistry*, Cambridge University Press, Cambridge, 2012.
7 P. Manikandan, J. Zhang and W. L. Hase, *J. Phys. Chem. A*, 2012, **116**, 3061–3080.
8 Y. Wang, H. Song, I. Szabó, G. Czakó, H. Guo and M. Yang, *J. Phys. Chem. Lett.*, 2016, **7**, 3322–3327.
9 J. Meyer and R. Wester, *Annu. Rev. Phys. Chem.*, 2017, **68**, 333–353.
10 T. J. Millar, C. Walsh and T. A. Field, *Chem. Rev.*, 2017, **117**, 1765–1795.
11 C. E. Dateo and D. C. Clary, *J. Chem. Soc., Faraday Trans. 2*, 1989, 1685–1696.
12 M. González, M. Gilibert, A. Aguilar and R. Sayós, *J. Chem. Phys.*, 1993, **98**, 2927–2935.
13 I. Szabó, A. G. Császár and G. Czakó, *Chem. Sci.*, 2013, **4**, 4362.
14 A. Li, Y. Li, H. Guo, K.-C. Lau, Y. Xu, B. Xiong, Y.-C. Chang and C. Y. Ng, *J. Chem. Phys.*, 2014, **140**, 011102.
15 H. Song, A. Li, H. Guo, Y. Xu, B. Xiong, Y. C. Chang and C. Y. Ng, *Phys. Chem. Chem. Phys.*, 2016, **18**, 22509–22515.
16 H. Song, A. Li, M. Yang and H. Guo, *Phys. Chem. Chem. Phys.*, 2017, **19**, 17396–17403.
17 B. Olasz, I. Szabo and G. Czako, *Chem. Sci.*, 2017, **8**, 3164–3170.
18 Y. Zhu, L. Tian, H. Song and M. Yang, *J. Chem. Phys.*, 2019, **151**, 054311.
19 N. Bulut, A. Aguado, C. Sanz-Sanz and O. Roncero, *J. Phys. Chem. A*, 2019, **123**, 8766–8775.
20 Q. Yao, M. Morita, C. Xie, N. Balakrishnan and H. Guo, *J. Phys. Chem. A*, 2019, **123**, 6578–6586.
21 C. M. Persson, M. De Luca, B. Mookerjea, A. O. H. Olofsson, J. H. Black, M. Gerin, E. Herbst, T. A. Bell, A. Coutens and B. Godard, *et al.*, *Astron. Astrophys.*, 2012, **543**, A145.
22 K. Beloy, M. G. Kozlov, A. Borschevsky, A. W. Hauser, V. V. Flambaum and P. Schwerdtfeger, *Phys. Rev. A: At., Mol., Opt. Phys.*, 2011, **83**, 062514.
23 O. Lakhmanskaya, M. Simpson, S. Murauer, M. Nötzold, E. Endres, V. Kokoouline and R. Wester, *Phys. Rev. Lett.*, 2018, **120**, 253003.
24 C. M. Persson, M. Hajigholi, G. E. Hassel, A. O. H. Olofsson, J. H. Black, E. Herbst, H. S. P. Müller, J. Cernicharo, E. S. Wirström and M. Olberg, *et al.*, *Astron. Astrophys.*, 2014, **567**, A130.
25 P. R. Roelfsema, F. P. Helmich, D. Teyssier, V. Ossenkopf, P. Morris, M. Olberg, R. Shipman, C. Risacher, M. Akyilmaz and R. Assendorp, *et al.*, *Astron. Astrophys.*, 2012, **537**, A17.
26 G. L. Pilbratt, J. R. Riedinger, T. Passvogel, G. Crone, D. Doyle, U. Gageur, A. M. Heras, C. Jewell, L. Metcalfe and S. Ott, *et al.*, *Astron. Astrophys.*, 2010, **518**, L1.
27 D. K. Bohme, R. S. Hemsworth and H. W. Rundle, *J. Chem. Phys.*, 1973, **59**, 77–81.
28 R. Otto, J. Mikosch, S. Trippel, M. Weidemuller and R. Wester, *Phys. Rev. Lett.*, 2008, **101**, 063201.

29 F. A. Gianturco, E. Yurtsever, M. Satta and R. Wester, *J. Phys. Chem. A*, 2019, **123**, 9905–9918.
30 T. B. Adler, G. Knizia and H.-J. Werner, *J. Chem. Phys.*, 2007, **127**, 221106.
31 G. Knizia, T. B. Adler and H.-J. Werner, *J. Chem. Phys.*, 2009, **130**, 054104.
32 K. Shao, J. Chen, Z. Zhao and D. H. Zhang, *J. Chem. Phys.*, 2016, **145**, 071101.
33 H. J. Werner, P. J. Knowles, G. Knizia, F. R. Manby and M. Schutz, *Wiley Interdiscip. Rev.: Comput. Mol. Sci.*, 2012, **2**, 242–253.
34 H. B. S. M. J. Frisch, G. E. Scuseria, M. A. Robb, J. R. Cheeseman, G. Scalmani, V. Barone, G. A. Petersson, H. Nakatsuji and X. M. Li, *Gaussian 09*, 2009.
35 M. A. Collins, *Theor. Chem. Acc.*, 2002, **108**, 313–324.
36 R. Chen, K. Shao, B. Fu and D. H. Zhang, *J. Chem. Phys.*, 2020, **152**, 204307.
37 L. M. Raff, R. Komanduri, M. Hagan and S. T. S. Bukkapatnam, *Neural Networks in Chemical Reaction Dynamics*, Oxford University Press, Oxford, 2012.
38 J. Li, B. Jiang and H. Guo, *J. Chem. Phys.*, 2013, **139**, 204103.
39 B. Jiang and H. Guo, *J. Chem. Phys.*, 2013, **139**, 054112.
40 Z. Xie and J. M. Bowman, *J. Chem. Theory Comput.*, 2010, **6**, 26–34.
41 Z.-H. Zhou, J. Wu and W. Tang, *Artif. Intell.*, 2010, **174**, 1570.
42 W. L. Hase, R. J. Duchovic, X. Hu, A. Komornicki, K. F. Lim, D. H. Lu, G. H. Peslherbe, K. N. Swamy, S. V. Linde and A. Varandas, VENUS96: A General Chemical Dynamics Computer Program. *QCPE Bulletin*, 1996.
43 D. A. Tasi, Z. Fábián and G. Czakó, *Phys. Chem. Chem. Phys.*, 2019, **21**, 7924–7931.
44 J. L. B. J. Zheng, R. Meana-Pañeda, S. Zhang, B. J. Lynch, J. C. Corchado, Y.-Y. Chuang, P. L. Fast, W.-P. Hu, Y.-P. Liu, G. C. Lynch, K. A. Nguyen, C. F. Jackels, A. F. Ramos, B. A. Ellingson, V. S. Melissas, J. Villa, I. Rossi, E. L. Coitino, J. Pu and T. V. Albu, *POLYRATE, version 9.7*, Department of Chemistry and Supercomputing Institute, University of Minnesota, 2007.
45 P. d. Mazo-Sevillano, A. Aguado and O. Roncero, *J. Chem. Phys.*, 2021, **154**, 094305.